Materials and Design 32 (2011) 1356–1366

Contents lists available at ScienceDirect

Materials and Design

journal homepage: www.elsevier.com/locate/matdes

Experimental investigations on the ballistic impact performances of cold rolled sheet metals

A. Durmuş [a,*], M. Güden [b], B. Gülçimen [a], S. Ülkü [a], E. Musa [c]

[a] Department of Mechanical Engineering, Uludağ University, Görükle, 16059 Bursa, Turkey
[b] Department of Mechanical Engineering, İzmir Institute of Technology, Gülbahçe Köyü, Urla, 35430 İzmir, Turkey
[c] Department of Electronic Engineering, Uludağ University, Görükle, 16059 Bursa, Turkey

ARTICLE INFO

Article history:
Received 3 May 2010
Accepted 9 September 2010
Available online 21 September 2010

Keywords:
Impact and ballistic
Film and sheet
Failure analysis

ABSTRACT

This study focuses on the ballistic performances of 1 and 2 mm-thick and 2 × 1 mm-thick cold rolled sheet metal plates against 9 mm standard NATO projectile. The velocity of the projectile before and after perforation, the diameter of the front face deformation, the depth of the crater and the diameter of the hole were measured. The fracture surfaces of the plates near the ballistic limit were also microscopically analyzed. The highest ballistic limit was found in 2 mm-thick plate (332 m s^{-1}) and the lowest in 1 mm-thick plate (97 m s^{-1}). While, the ballistic limit of 2 × 1 mm-thick plate decreased to 306 m s^{-1}. Typical failure mechanism of the projectile was the flattening and mushrooming at relatively low velocities and the separation from the jacket at relatively high velocities. In accord with the ballistic limits, 2 mm-thick target plate exhibited the highest hardness value. Microscopic investigations showed the significant reductions in the grain size of the targets after the test.

1. Introduction

Cold rolled sheet metals are commercially available cost effective materials with quite wide range of applications. At the same time, they have the potentials to be used in the structure of the armor vehicles for the protection against small caliber soft jacketed projectiles. In this specific application, the intended ballistic protection naturally vanishes when the ballistic impact damage/the target failure emerges. Therefore, the target damage initiation and the subsequent emerge of the target fracture are two important phenomena which should be taken into account when assessing the performances of the ductile targets against ballistic treats. In a previous study, Børvik et al. [1] investigated the fracture and penetration of a projectile in a Weldox 460 E steel plate. Chen et al. [2] developed an analytical model for the localized shear zone formation in a Weldox 460 E steel plate. The perforation of ductile metal targets by a conical indenter was investigated by Nazeer et al. [3]. The number and size of petals formed were reported to depend on the sheet metal thickness, sheet metal mechanical properties, indenter angle, anisotropy and the indentation speed. Liu and Stronge [4] showed when a mild steel plate was struck by a flat-ended missile at a velocity near the ballistic limit at a normal angle of obliquity, the failure changed from dishing to plugging as the ratio of the plate thickness to missile radius increased. It was also shown in the same study that the part of the initial missile kinetic energy absorbed by the global deformation (dishing) was larger for the soft missiles since the missile mushrooming increased the plug diameter and the mushroomed nose had a larger curvature at the periphery of the contact region, reducing the shear strain in the hinge band. The formation of multiple necks and cracks around perforations in ductile metals was further studied by Atkins et al. [5]. The numbers of plane-strain radial necks formed by conical and round-ended projectiles into flat targets were determined. Segletes [6] investigated the penetration of ductile targets impacted by a hemispherical-nosed tungsten projectile at the erosion-threshold velocity. In another experimental study, the ballistic resistance and damage formation of the heat treated steel targets with different thicknesses, hole diameters and target mounting was investigated [7]. Rusinek et al. [8] studied experimentally and numerically the failure of mild steel sheets subjected to normal impact by hemispherical projectiles. Klepaczko et al. [9] have recently simulated the projectile impact of DH-36 and Weldox 460-E structural steels using three different material models. The Rusinek–Klepaczko model was shown to be in good agreement with experimental results. Dean et al. [10] modeled the absorbed impact energies of the steel plates using Johnson–Cook plasticity algorithm.

Despite many experimental and numerical investigations on the perforation and penetration of the ductile metal targets by rigid projectiles, few experimental studies have concentrated on

* Corresponding author. Tel.: +90 224 2941989; fax: +90 224 2941903.
E-mail address: adurmus@uludag.edu.tr (A. Durmuş).

0261-3069/$ - see front matter © 2010 Elsevier Ltd. All rights reserved.
doi:10.1016/j.matdes.2010.09.016

Table 1
The chemical compositions of H320LA target sheets (wt.%).

1 mm	C 0.058	Si 0.018	Mn 0.341	P 0.011	S 0.014	Cr 0.023	Ni 0.023	Mo 0.001	Cu 0.012
	Al 0.034	Ti 0.001	V 0.001	Nb 0.030	W 0.006	Co 0.001	Sn 0.001	Pb 0.002	Sb 0.010
2 mm	C 0.083	Si 0.008	Mn 1.063	P 0.010	S 0.005	Cr 0.021	Ni 0.031	Mo 0.002	Cu 0.019
	Al 0.064	Ti 0.002	V 0.002	Nb 0.053	W 0.005	Co 0.008	Sn 0.001	Pb 0.002	Sb 0.013

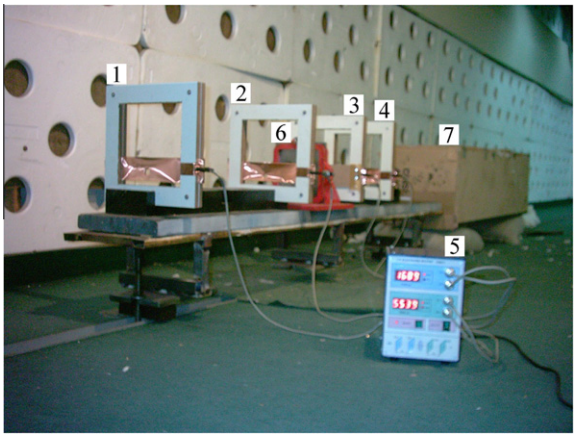

Fig. 1. Experimental projectile impact set-up: (1) first trigger for initial velocity, (2) second trigger for initial velocity, (3) first trigger for residual velocity, (4) second trigger for residual velocity, (5) timer, (6) rigid frame for target and (7) bullet holder box.

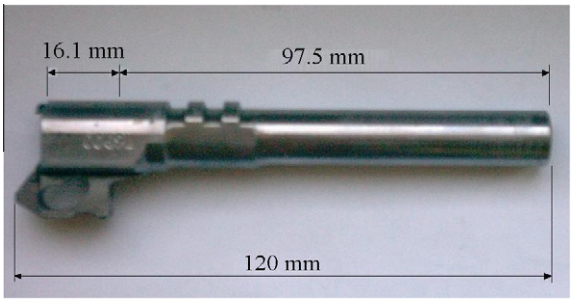

Fig. 3. Barrel used in the shutting system.

Fig. 4. Projectile of the 9 mm × 19 Parabellum cartridge and its cross sections.

the damage formation and the failure in the ductile metal targets struck by lead core-brass jacketed bullets. The aim of present study is therefore to investigate the protection capability of cold rolled steel sheets widely used in the automotive industry against 9 mm standard NATO projectiles.

2. Experimental

2.1. Materials

Low carbon cold rolled H320LA (DIN EN 10268–99) steel sheets were received in 1 and 2 mm thicknesses. The tested steel is a low carbon alloy steel (Table 1); therefore, the strength is mainly driven by the applied cold rolling process rather than alloying. The tensile tests were performed on the tensile tests coupons parallel to the rolling direction in accord with ASTM E8/E8M-09

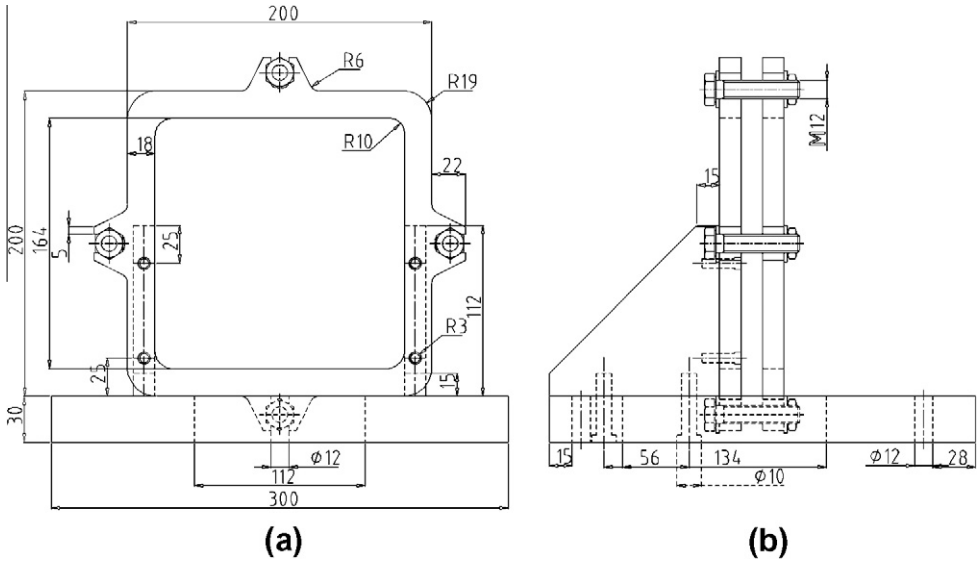

Fig. 2. The frame used in the projectile impact test, (a) front and (b) side views.

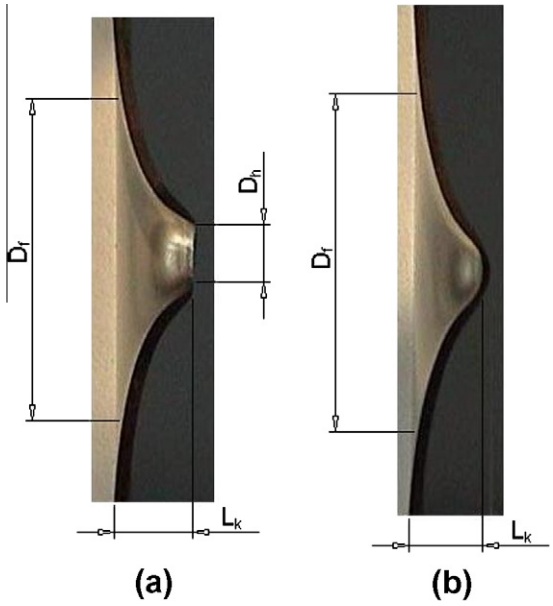

Fig. 5. Impacted plate, showing D_f (front face deformation), L_k (crater depth) and D_h diameter of the hole after penetration: (a) perforated and (b) nonperforated.

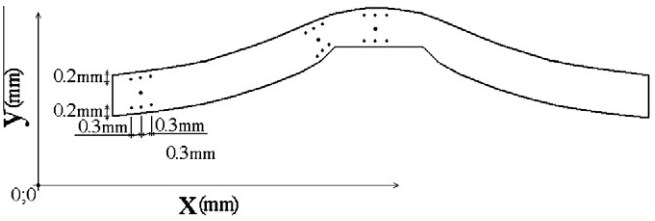

Fig. 6. Crater microhardness measurements locations in nonperforated plates.

standard [11]. The samples were tested within the quasi-static strain rate regime of 1.33×10^{-4} and 6.6×10^{-2} s^{-1}.

2.2. Experimental set-up

The projectile impact test apparatus used in the ballistic tests is shown in Fig. 1 and mainly consists of trigger systems for the measurement of the initial and residual velocities of the projectile (1, 2, 3 and 4), a timer connected to the triggers (5), a rigid frame for the target insert (6) and a bullet holder box (7). The targets were clamped at the ends to the target frame as depicted in Fig. 2, leaving a target area of 164 mm × 164 mm. The used barrel and its dimensions are shown in Fig. 3. The projectile was a 9 mm × 19 Parabellum cartridge with varying amounts of Ball Powder® gunpowder. The weight of the full metal jacketed projectile is 8 g and the core and the jacket are made from 2 wt.% antimony-lead alloy and brass (CuZn36), respectively (Fig. 4). The velocity of the projectile before and after the ballistic test was measured using a velocity measurement set-up [12]. Depending on the amount of the gunpowder used in the cartridge, the projectile velocity varied between 69 and 377 m s^{-1}. The followings were measured in the perforated and nonperforated plates: the diameter of the front face deformation (D_f), crater depth (L_k) and diameter of the hole (D_h) after penetration (Fig. 5). The values of D_f and L_k were measured using a Conturograph C4P device, whereas D_h values were determined using a Microtecnica projector mirror. The accuracy of the measurements was within ±45 μm and ±5 μm for the Conturograph C4P device and the Microtecnica projector, respectively.

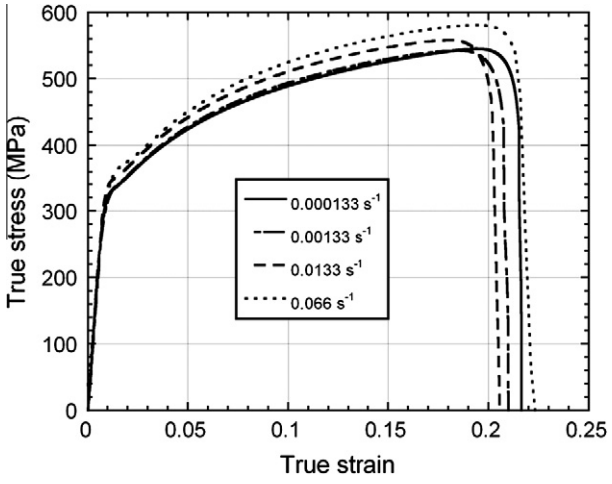

Fig. 7. Quasi-static true tensile stress–strain curves of 2 mm-thick steel at different strain rates.

The specimens for the optical investigations were prepared metallographically through grinding and polishing. The polished surfaces of the samples were then etched using a 3% nital solution. Microscopic observations on the perforated sections and plugs were performed using a scanning electron microscope (SEM). The microhardness tests were conducted on the crater region, at the beginning of the crater region and on the intense deformation bands as shown in Fig. 6. The hardness measurements were performed at a distance of 0.2 mm from the edges of the tested sheets at 0.3 mm intervals. The microhardness values were reported as the average of six hardness measurements.

3. Results and discussions

True stress–strain curves of the tested sheet steel, parallel to the extrusion direction, at increasing quasi-static strain rates are shown in Fig. 7. The flow stresses of the tested steel parallel to the extrusion direction increase with increasing the strain rate within the studied strain rate regime, showing clearly a strain rate dependent flow stress and yield and tensile strength behavior (Fig. 7).

The initial and residual velocities of the projectile, plug mass, projectile failure mode, final length of the projectile, projectile mushrooming/flatting diameter, D_h, L_k and D_f for 1 mm-thick, 2 mm-thick and 2 × 1 mm-thick plates are tabulated sequentially in Tables 2–4, respectively. The pictures of 1 mm, 2 mm and 2 × 1 mm-thick targets and the projectiles after ballistic test at different projectile velocities are shown in Figs. 8–10, respectively. The perforation of 1 mm-thick plate occurs at the projectile velocities above 97 m s^{-1} as tabulated in Table 2. At 97 m s^{-1}, the target is essentially partially perforated (Test #13 in Table 3 and Fig. 8d); however, as the target is breached at this projectile velocity (the light passes through it), the ballistic limit is taken as 97 m s^{-1}. A very similar approach for the ballistic limit determination was also previously reported in Ref. [13]. The projectile nose flattens around the ballistic limit (Table 2, F and Figs. 8c–f), while at increasing impact velocities above the ballistic limit, the projectile is partially mushroomed (Table 2, M_p and Fig. 8a and b). For the complete perforation, the plug mass and plug thickness are measured 0.30 ± 0.07 g and 0.50 ± 0.04 mm, respectively. At the highest impact velocity, 376.7 m s^{-1}, the plug diameter is 7.71 mm. This value is found to decrease with decreasing impact velocities, being equal to 5.35 mm at 136.9 m s^{-1} projectile velocity.

The ballistic limit of 2 mm-thick target is calculated by averaging the highest projectile velocity at which no perforation occurs

Table 2
Ballistic test results of 1 mm-thick plate.

Test No.	V_i (m s^{-1})	V_r (m s^{-1})	Plug mass (g)	Projectile failure type	Projectile final length (mm)	Projectile mushrooming or flatting diameter (mm)	D_h (mm)	L_k (mm)	D_f (mm)
#1	377	339	0.4	M_p	13.44	9.53	9.41	5.72	23.10
#2	370	336	0.3	M_p	13.44	9.50	9.36	5.79	29.82
#3	341	311	0.3	M_p	13.62	9.40	9.28	6.16	25.13
#4	329	291	0.3	M_p	13.60	9.41	9.28	6.06	36.03
#5	311	270	0.3	M_p	13.60	9.30	9.18	6.15	27.09
#6	300	262	0.4	M_p	13.48	9.35	9.28	6.33	30.21
#7	272	229	0.3	M_p	13.63	9.19	9.03	6.41	28.06
#8	260	216	0.3	M_p	13.38	9.33	9.24	6.57	30.36
#9	238	192	0.3	M_p	13.58	9.22	9.15	6.99	37.77
#10	211	158	0.2	M_p	13.64	9.12	9.02	6.90	36.04
#11	153	79	0.2	F	14.70	5.94	8.71	7.13	39.58
#12	137	35	0.2	F	14.94	5.74	8.65	7.30	41.79
#13	97	–	–	F	14.70	5.23	–	5.91	49.32
#14	78	–	–	F	14.91	4.94	–	4.31	55.35
#15	71	–	–	F	15.01	4.62	–	3.60	42.73

Table 3
Ballistic test results of 2 mm-thick plate.

Test No.	V_i (m s^{-1})	V_r (m s^{-1})	Plug mass (g)	Projectile failure type	Projectile final length (mm)	Projectile mushrooming or flatting diameter (mm)	Diameter of lead core (mm)	Length of lead core (mm)	D_h (mm)	L_k (mm)	D_f (mm)
#1	371	224	0.6	S	–	–	10.62	*6.49*	10.59	11.93	71.82
#2	363	209	0.6	S	–	–	10.37	*6.39*	10.29	11.66	63.84
#3	338	125	0.5	S	–	–	9.11	5.52	9.06	12.57	76.56
#4	325	–	–	S	–	–	8.25	8.40	–	12.81	89.89
#5	307	–	–	S	–	–	21.43	5.71	–	11.79	89.37
#6	287	–	–	S	–	–	21.91	5.19	–	10.41	78.78
#7	266	–	–	S	–	–	19.91	4.75	–	9.02	78.37
#8	259	–	–	S	–	–	21.73	4.81	–	8.75	83.43
#9	232	–	–	S	–	–	18.50	5.32	–	7.39	75.07
#10	218	–	–	S	–	–	19.15	5.31	–	6.75	81.73
#11	116	–	–	M_p	12.70	9.65	–	–	–	2.73	50.90
#12	103	–	–	M_p	12.96	9.24	–	–	–	2.25	46.79
#13	93	–	–	M_p	13.13	9.05	–	–	–	1.89	45.93
#14	69	–	–	F	13.81	6.81	–	–	–	1.08	37.95

Table 4
Ballistic test results of 2 × 1 mm-thick plate.

Test No.	V_i (m s^{-1})	V_r (m s^{-1})	Plug mass (g)		Projectile failure type	Projectile final length (mm)	Projectile mushrooming or flatting diameter (mm)	Diameter of lead core (mm)	Length of lead core (mm)	D_h (mm)		L_k (mm)		D_f (mm)	
			Front plate	Back plate						Front plate	Back plate	Front plate	Back plate	Front plate	Back plate
#1	373	222	0.4	0.4	S	–	–	10.21	7.75	12.89	11.81	10.91	11.98	66.97	68.86
#2	363	183	0.4	0.4	S	–	–	11.39	8.31	12.29	11.35	11.28	12.28	70.25	83.64
#3	335	120	0.4	0.4	S	–	–	10.71	7.42	11.49	10.57	10.97	12.14	70.38	71.24
#4	324	104	0.4	0.5	S	–	–	10.15	8.34	11.23	10.30	10.83	11.82	71.11	76.59
#5	306	–	–	–	M_d	12.26	15.06	–	–	–	–	9.94	11.88	74.71	83.59
#6	301	–	–	–	M_d	12.72	14.98	–	–	–	–	9.86	11.56	82.21	78.01
#7	300	–	–	–	M_d	11.53	15.31	–	–	–	–	9.00	10.93	80.47	76.39
#8	263	–	–	–	M_d	10.19	14.66	–	–	–	–	8.95	8.78	69.24	80.92
#9	251	–	–	–	M_d	11.82	15.75	–	–	–	–	8.13	7.90	70.41	67.97
#10	235	–	–	–	M_d	9.93	14.30	–	–	–	–	7.56	7.31	80.46	81.09
#11	211	–	–	–	M_d	9.62	14.26	–	–	–	–	6.07	6.06	62.34	76.20
#12	160	–	–	–	M_d	11.64	11.53	–	–	–	–	4.90	4.74	58.33	60.57
#13	117	–	–	–	M_p	12.84	9.50	–	–	–	–	3.56	3.62	54.26	61.60
#14	94	–	–	–	F	13.49	7.65	–	–	–	–	3.06	2.92	67.54	66.06
#15	90	–	–	–	F	13.60	7.54	–	–	–	–	2.88	2.47	59.11	39.47

(Table 3, Test 4) and the lowest projectile velocity at which the complete perforation of the target occurs (Table 3, Test 3). This gives a ballistic limit of 332 m s^{-1} for 2 mm-thick plate. Since the projectile separates from the jacket in the ballistic testing of 2 mm-thick targets (Fig. 9a, b and d), the velocity of the lead core is taken as the residual velocity. It is also noted, although 2 mm-thick target is perforated at a velocity of 325 m s^{-1}, the projectile remains attached to the target (Fig. 9c). The projectile deformation in these target plates is the flattening and mushrooming at relatively low velocities (Fig. 9e and f) and the separation from the

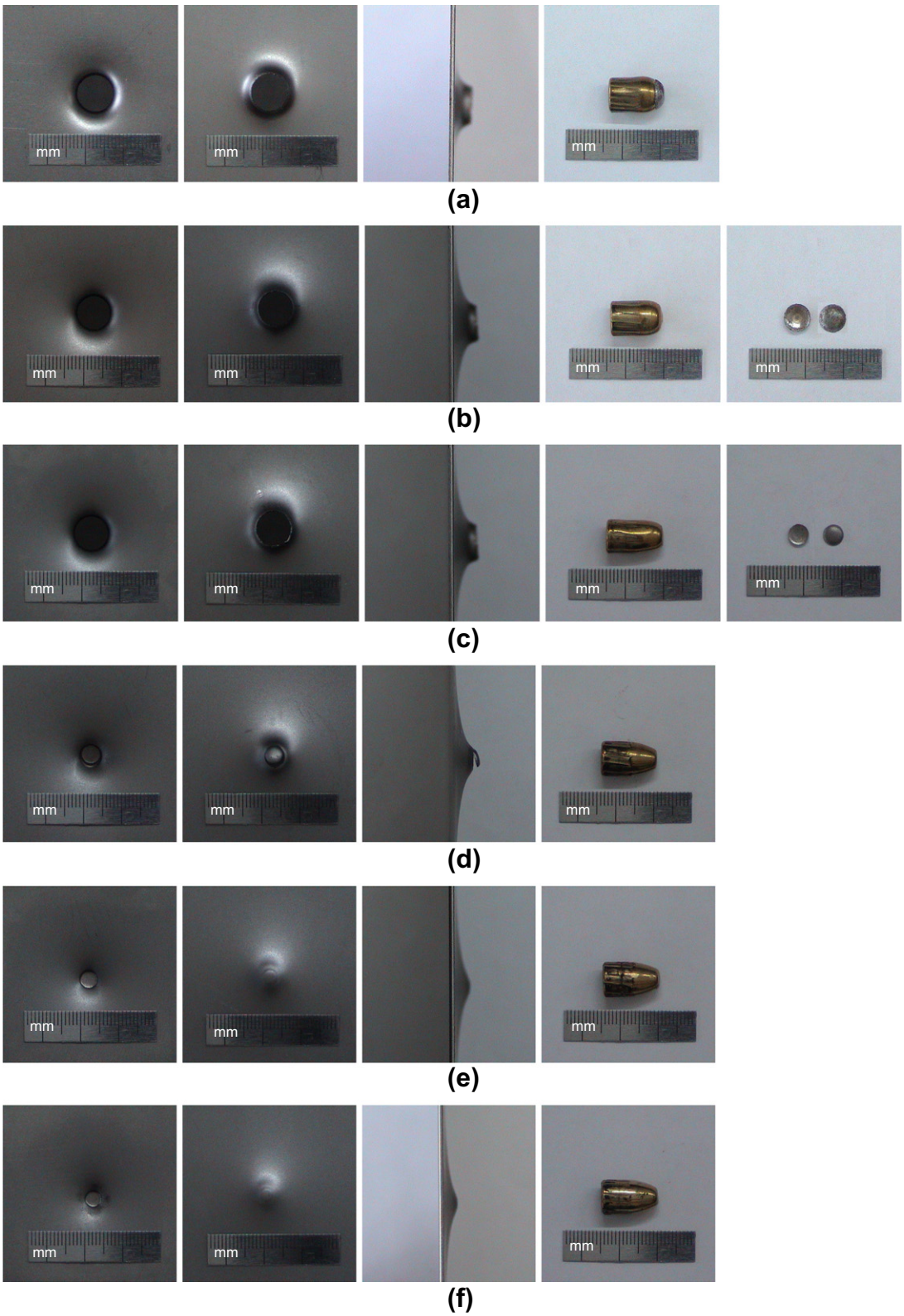

Fig. 8. Front and back face and side pictures of 1 mm-thick plates and projectile: (a) $V_i = 377 \pm 5.6$ m s^{-1}, $V_r = 339 \pm 10.2$ m s^{-1}; (b) $V_i = 305 \pm 4.5$ m s^{-1}, $V_r = 269 \pm 8.0$ m s^{-1}; (c) $V_i = 137 \pm 2.0$ m s^{-1}, $V_r = 35 \pm 1.0$ m s^{-1}; (d) $V_i = 97 \pm 1.4$ m s^{-1}, $V_r = 0$ m s^{-1}; (e) $V_i = 78 \pm 1.1$ m s^{-1}, $V_r = 0$ m s^{-1}; (f) $V_i = 71 \pm 1.0$ m s^{-1}, $V_r = 0$ m s^{-1}.

jacket at relatively high velocities. The mass, thickness and diameter of the plug of 2 mm-thick plates are measured sequentially 0.60 ± 0.07 g, 1.00 ± 0.08 mm and 8.95 ± 1.40 mm.

In 2 × 1 mm-thick plates, although the plug in Test 4 (Table 4) is completely separated from the front plate, it twists through the back plate (not entirely broken) as shown in Fig. 10b. The partial perforation of the front and back plate occurs in Test 5 (Fig. 10c). Therefore, the ballistic limit of 2 × 1 mm-thick plates is taken as 306 m s^{-1}. The projectile failure at and near the ballistic limit is dominantly mushrooming (M_d) (Fig. 10c–e). In addition, the plugs

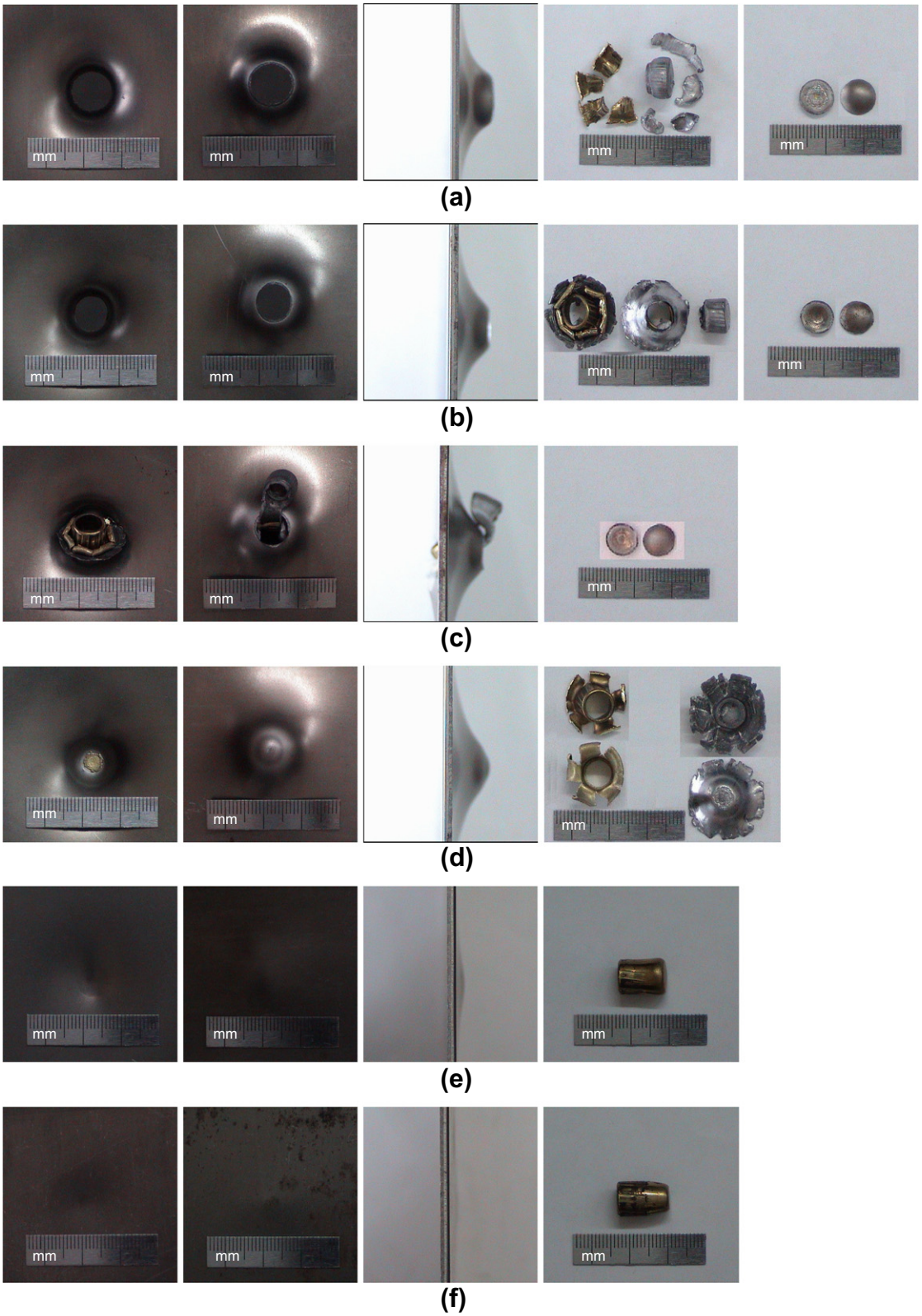

Fig. 9. Front and back face and side pictures of impacted 2 mm-thick plates and projectile: (a) $V_i = 371 \pm 5.6$ m s^{-1}, $V_r = 224 \pm 6.6$ m s^{-1}; (b) $V_i = 338 \pm 5$ m s^{-1}, $V_r = 125 \pm 3.7$ m s^{-1}; (c) $V_i = 325 \pm 4.8$ m s^{-1}, $V_r = 0$ m s^{-1}; (d) $V_i = 307 \pm 4.6$ m s^{-1}, $V_r = 0$ m s^{-1}; (e) $V_i = 116 \pm 1.7$ m s^{-1}, $V_r = 0$ m s^{-1}; (f) $V_i = 69 \pm 1.0$ m s^{-1}, $V_r = 0$ m s^{-1}.

are observed to be symmetrical in shape above the ballistic limit (Fig. 10b) and become asymmetric at increasing impact velocities. The mass, thickness and diameter of the plugs of the front and back plate are found to be very similar to each other. The plug mass (0.40 ± 0.04 g) and thickness (0.50 ± 0.04 mm) of 2×1 mm-thick plate are very similar to those of 1 mm-thick plate, while the diameter of the plugs (9.23 ± 0.18 mm) is larger than that of 1 mm-thick plate.

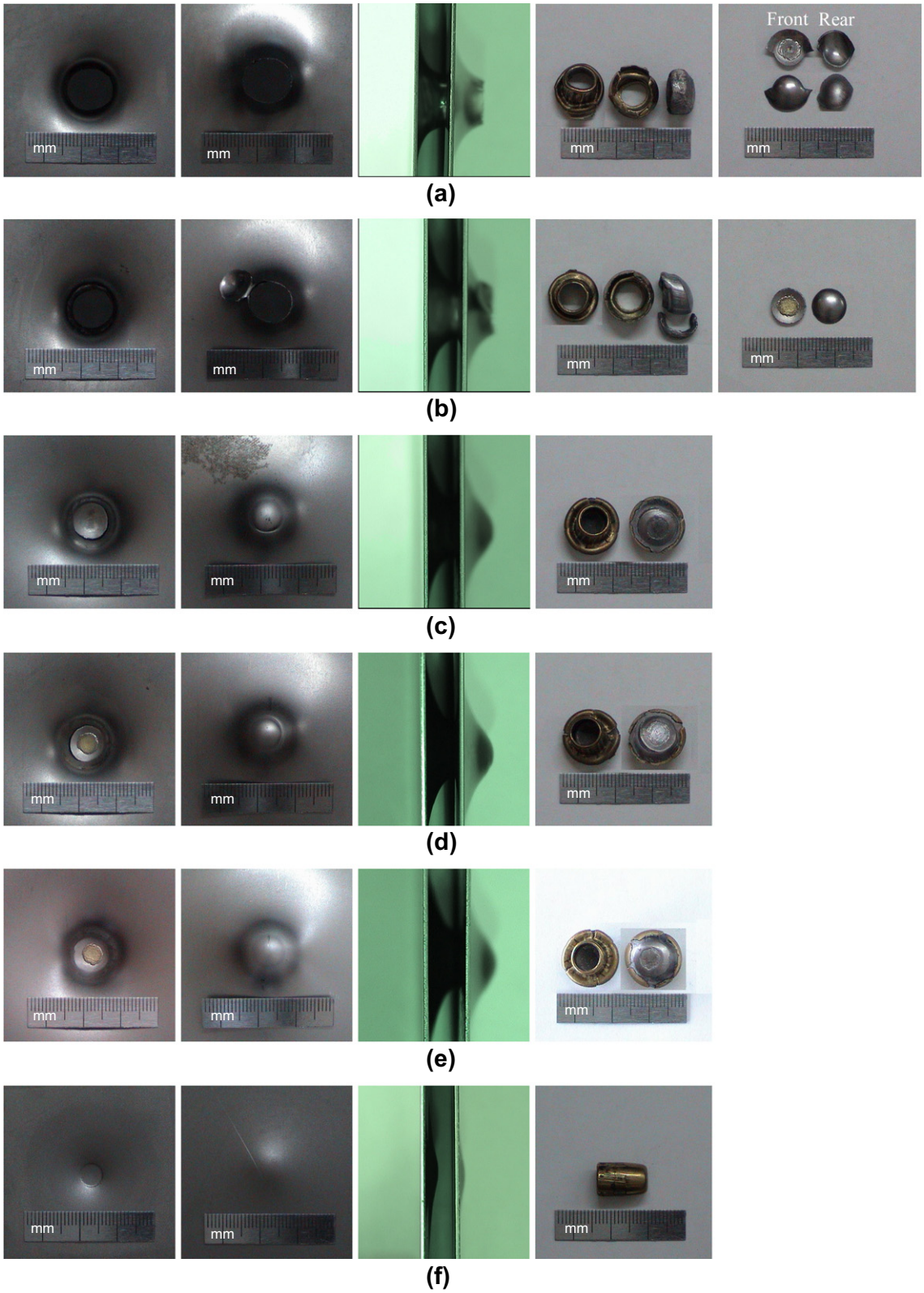

Fig. 10. Front and back face and side pictures of impacted 2 × 1 mm-thick plates and projectile: (a) $V_i = 373 \pm 5.6$ m s^{-1}, $V_r = 222 \pm 6.6$ m s^{-1}; (b) $V_i = 324 \pm 4.8$ m s^{-1}, $V_r = 104 \pm 3.0$ m s^{-1}; (c) $V_i = 306 \pm 4.5$ m s^{-1}, $V_r = 0$ m s^{-1}; (d) $V_i = 301 \pm 4.5$ m s^{-1}, $V_r = 0$ m s^{-1}; (e) $V_i = 300 \pm 4.5$ m s^{-1}, $V_r = 0$ m s^{-1}; (f) $V_i = 90 \pm 1.3$ m s^{-1}, $V_r = 0$ m s^{-1}.

The experimental residual projectile velocity of the plates as function of impact velocity is shown in Fig. 11. As noted in the same figure, the residual velocities approach the residual velocity line at increasingly high impact velocities. Here, the residual velocity line is the asymptotic response to a zero thickness target according to Børvik et al. [14]. The projectile velocity differences $(V_i - V_r)$ are further noted to reach maximum values at the lowest perforation velocities; thereafter, the differences decrease abruptly

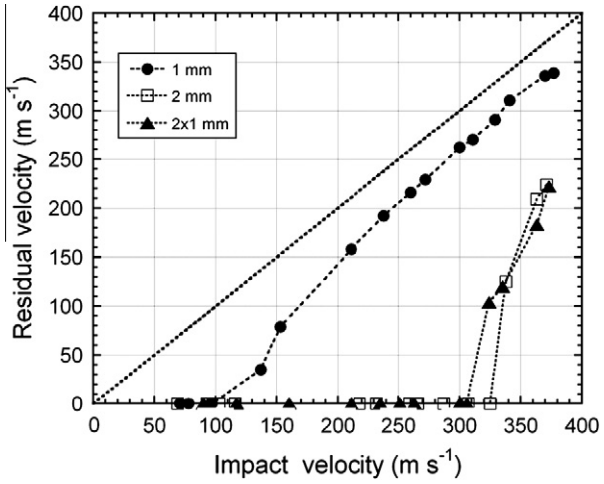

Fig. 11. Projectile residual velocity as a function of impact velocity.

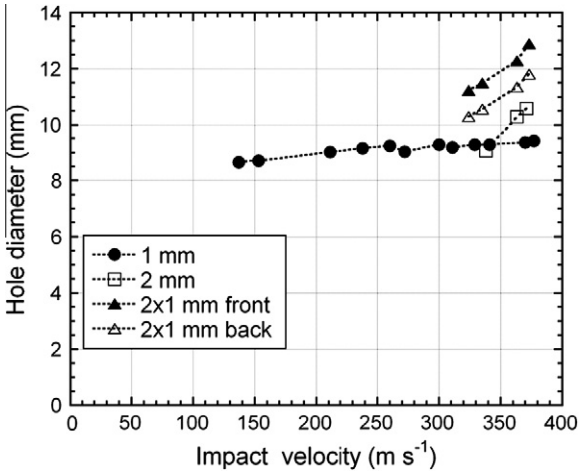

Fig. 13. Hole diameter vs. projectile impact velocity.

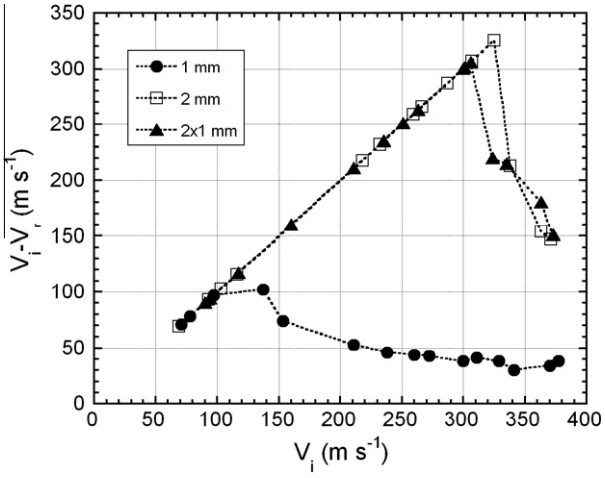

Fig. 12. Projectile velocity difference vs. projectile velocity.

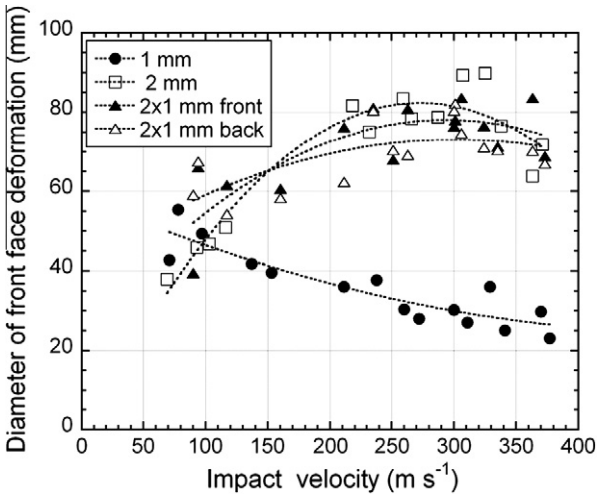

Fig. 14. Diameter of front face deformation (D_f) as function of impact velocity.

(Fig. 12). Because of this, the amount of energy absorptions by the deformation of the projectile and the target decrease as the projectile velocity increases. Fig. 13 shows the variation of the hole diameter of the plates as function of projectile impact velocity. The hole diameter is found to be larger than that of the projectile (9 mm) in 2 mm and 2 × 1 mm-thick plate and increases almost linearly with projectile impact velocity as seen in Fig. 13. Furthermore, the hole diameter of the front plate is larger than that of the back plate in 2 × 1 mm-thick plates. The difference between the hole diameters of the front and back plate is measured 0.73 mm at the lowest perforation velocity (324 m s^{-1}), while it increases to 1.08 mm when the projectile velocity increases to 373 m s^{-1}. It is also noted in the same figure that although the hole diameter in 1 mm-thick plate is larger than that of the projectile at the impact velocities higher than 211 m s^{-1}, it decreases below that of the projectile at lower impact velocities. This is an expected result as the elastic deformation and the spring back of the target and the set-groves of the projectile become more effective at relatively low perforation velocities.

The variations of the diameter of the front face deformation (D_f) and the crater depth (L_k) with the impact velocity are shown in Figs. 14 and 15, respectively. In 2 mm and 2 × 1 mm-thick plate, the diameter of front face deformation increases with increasing projectile impact velocity up to the ballistic limit; then, decreases

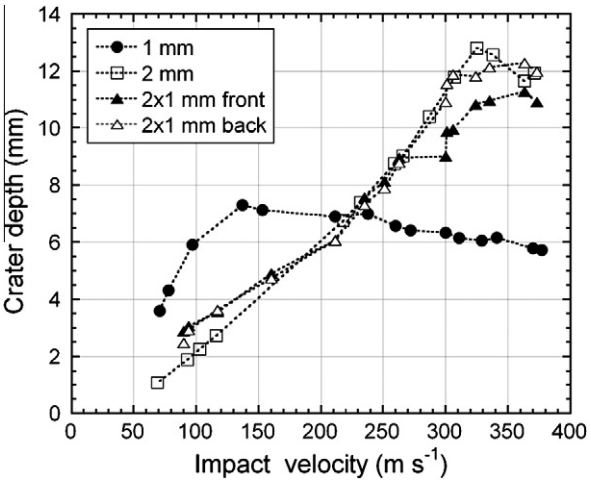

Fig. 15. The crater depth (L_k) as function of impact velocity.

slightly above the ballistic limit as seen in Fig. 14. In contrast to 2 mm and 2 × 1 mm-thick plate, the diameter of front face deformation in 1 mm-thick plate decreases with increasing impact

velocity. Within the investigated impact velocities, the crater depth of the plates increases almost linearly with impact velocity, up to ~325 m s^{-1}, except 1 mm-thick plates. The crater depth in 1 mm-thick plate increases sharply with increasing projectile velocity till about 150 m s^{-1} and then it gradually decreases. The front face deformation of the back plate in 2 × 1 mm-thick plate is also noted to be higher than that of the front plate. On the other hand, there is no notable difference in the crater depth between the front and back plates.

The microhardness values of the craters of the plates tested at the projectile velocities below the ballistic limits are tabulated in Table 5. The maximum microhardness in all tested plates was found in the intense deformation band. The increase in the microhardness values in the deformation band is approximately 49%, 47%, 58% and 47% in 1 mm-thick, 2 mm-thick, 2 × 1 mm-thick front plate and 2 × 1 mm-thick back plate, respectively. The increase in the microhardness values of the tested plates is attributed to the excessive deformation and the associated strain hardening behavior of the steel plates. As tabulated in Table 5 and 2 mm-thick target has the highest hardness, as it has the highest ballistic limit. The lowest hardness, on the other hand, was found at the beginning of the crater region in all tested targets. It is further noted that the hardness of the intense deformation region of the front plate of 2 × 1 mm-thick target is higher than that of the back plate and 1 mm-thick plate, while the hardnesses of the front and back plate at the beginning of the crater region and in the crater hill region are found very much similar.

The microstructure of the target material shows the typical microstructure of a low carbon steel, composing of mainly ferrite grains and uniformly distributed pearlitic regions. Fig. 16a–b shows the optical micrographs of the polished and etched cross sections of a 2 × 1 mm-thick target plate in the crater, at the beginning of the crater, in the intense deformation and in the crater hill region, respectively. It is observed that the grain sizes of the tested

Table 5
Microhardness of the craters at the maximum nonperforation impact velocity.

Target	Impact velocity (m s^{-1})	Region	x (mm)	y (mm)	Microhardness (HV_1)
1 mm (141 ± 4 HV_1)	78 ± 1.1	Hill	24.66	6.39	161 ± 6
		Intense deformation band	22.79	5.78	210 ± 5
		Crater beginning	15.58	3.95	147 ± 2
2 mm (158 ± 4 HV_1)	307 ± 4.6	Hill	44.95	13.46	222 ± 8
		Intense deformation band	41.87	12.71	232 ± 5
		Crater beginning	33.95	7.72	175 ± 4
2 × 1 mm Front plate(141 ± 4 HV_1)	300 ± 4.5	Hill	40.24	9.38	203 ± 3
		Intense deformation band	35.71	8.16	223 ± 6
		Crater beginning	30.28	4.17	177 ± 7
2 × 1 mm Rear plate (141 ± 4 HV_1)	300 ± 4.5	Hill	38.20	11.26	203 ± 4
		Intense deformation band	34.14	9.99	207 ± 7
		Crater beginning	29.28	6.60	180 ± 7

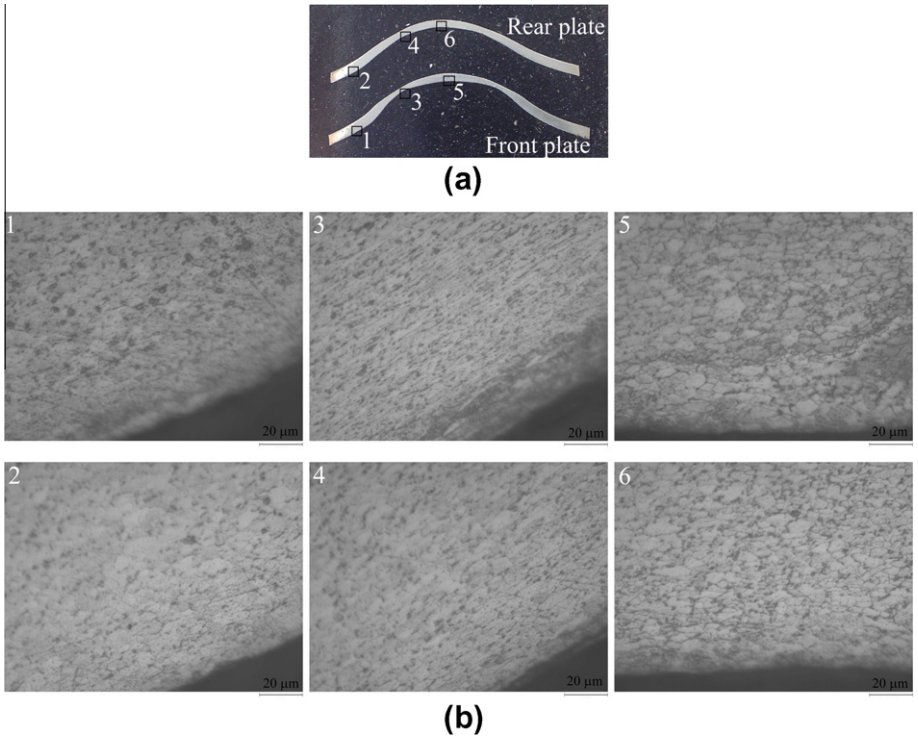

Fig. 16. Optical micrographs: (a) cross sections of target plates close to perforation of 2 × 1 mm-thick target; (b) microstructures of the crater beginning, intense deformation, and crater hill region of front and back plate.

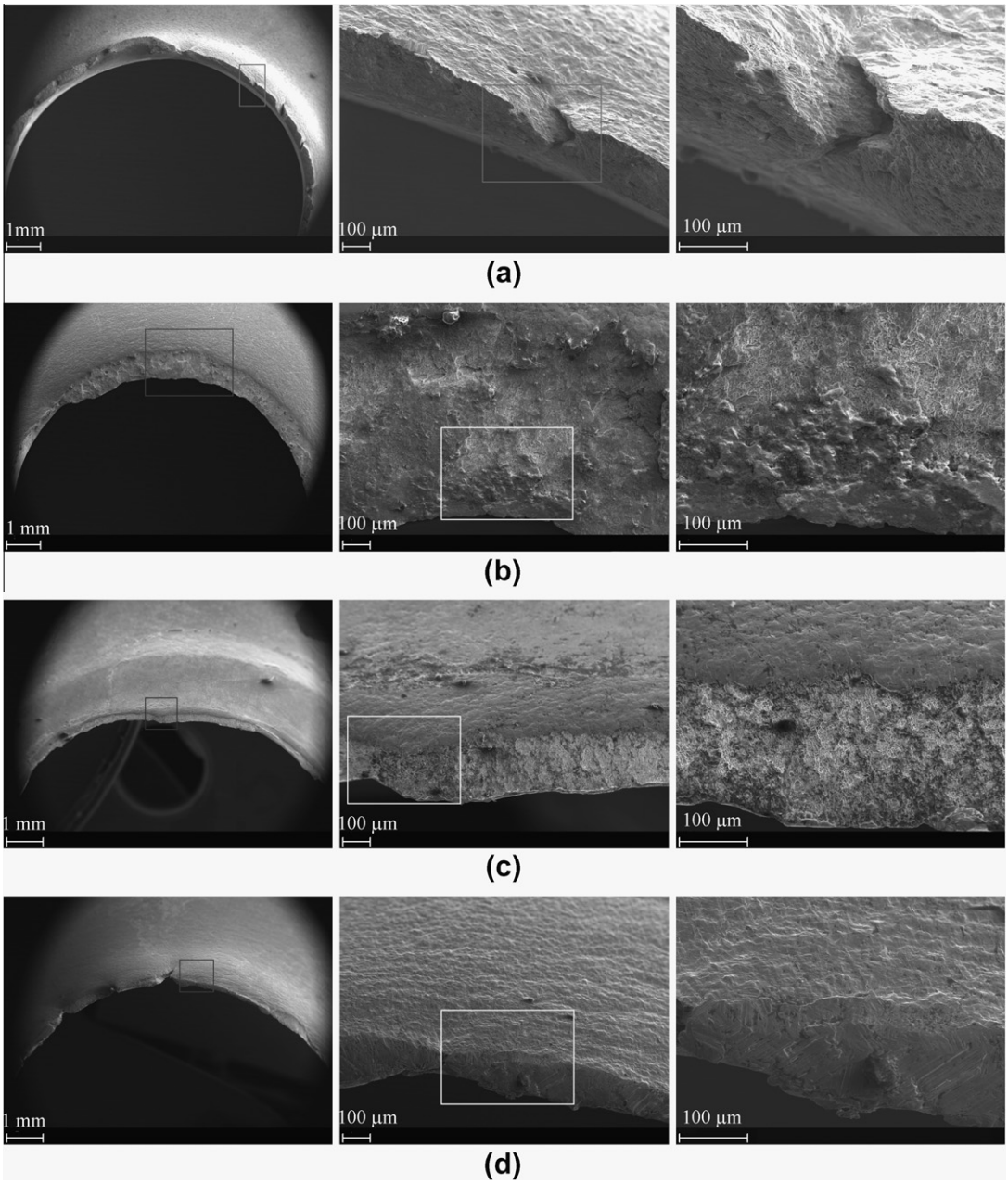

Fig. 17. SEM micrographs of the plates impacted near the ballistic limit: (a) 1 mm-thick target (V_s = 137 ± 2.0 m s^{-1}); (b) 2 mm-thick target (V_s = 325 ± 4.8 m s^{-1}); (c) front plate of 2 × 1 mm-thick target; (d) back plate of 2 × 1 mm-thick target (324 ± 4.8 m s^{-1}).

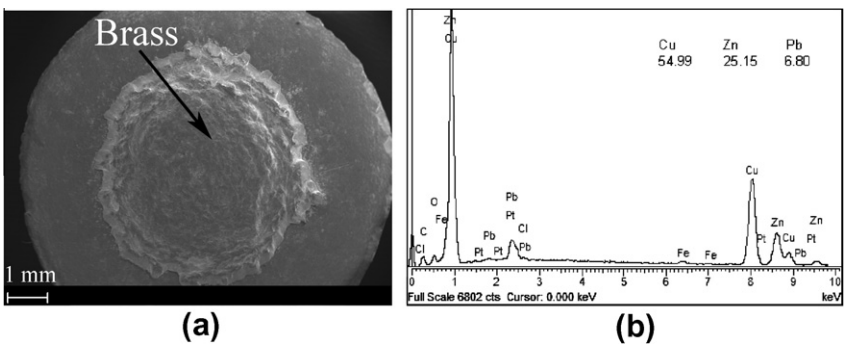

Fig. 18. (a) SEM image of the welded brass with a plug and (b) energy dispersive X-ray (EDX) analysis of the brass on plug surface.

targets significantly decreased. It is further noted that the grain size reduction in the crater hill is more intensive than the beginning of the crater region. The deformation of the grains is further observed to intensify towards the back surface of the targets.

The SEM micrographs of the perforated plates, near the ballistic limit, are shown in Fig. 17a–d for 1 mm-thick, 2 mm-thick and 2×1 mm-thick front and back plate, respectively. In 1 mm-thick plate, no molten metal is observed on the fracture surface (Fig. 17a). When the tensile stress on the back surface in these plates exceeds the ultimate stress, the crack forms randomly and propagates to the front surface and then the ductile failure occurs. The failure and plug formation result from the excessive deformation induced by the plastic bending, stretching and necking. However, partial melting on the fracture surface is observed in 2 mm-thick target (Fig. 17b). Relatively high deformation rates in these plates with the increased ballistic limit results in excessive increases in the temperature of impacted region, leading to the development of the adiabatic shear bands. Dimples and cleavage type of fracture are observed on the fracture surface of the front plate of 2×1 mm-thick target (Fig. 17c). The ductile failure of the front plate is partially attributed to the resistance of the back plate to the plugging of the front plate. The plug formed in the front plate punches the back plate, leading to the progression of the relatively flat fracture surfaces as seen in Fig. 17d). In addition, the jacket of projectile (brass) is noted to weld to the target surface near the ballistic limit. The EDX analysis of the impact site confirms the presence of Cu and Zn (Fig. 18).

The reduced ballistic limit of the double layer target (2×1 mm) as compared with single layer target of the same thickness (2 mm) was found to agree with the previous studies on layered targets. That is single targets are more effective than layered or laminated targets of the same total thickness [15–18]. The use of thicker backing plate and the appropriate standoff distance of the two plates were further shown to improve the performance of the layered targets [19]. The reduction of the thickness of the layers was also shown to reduce the ballistic limit of layered targets [20]. Furthermore, no effect of the anisotropy of the cold rolled sheet plates on the failure modes and the ballistic limits of the tested plates are detected. The terminal ballistic properties and the plug formation of the plates depend largely on the plate thickness and the configuration, mechanical properties of the target material and projectile velocity.

4. Conclusions

The highest ballistic limit was found in 2 mm-thick plate, 332 m s^{-1}, and the lowest in 1 mm-thick plate, 97 m s^{-1}. The ballistic limit of 2×1 mm-thick plate; however, reduced to 306 m s^{-1}. Typical projectile deformation was the flattening and mushrooming at relatively low velocities and the separation from the jacket at relatively high velocities. In accord with the ballistic limits, 2 mm-thick target showed the highest hardness. Reductions in grain size were observed after the ballistic test in all tested targets. The failure and plug formation were found to result from the excessive deformation induced by plastic bending, stretching and necking of the targets.

References

[1] Børvik T, Hopperstad OS, Berstad T, Langseth M. A computational model of viscoplasticity and ductile damage for impact and penetration. Eur J Mech A/Solids 2001;20:685–712.
[2] Chen XW, Li QM, Fan SC. Initiation of adiabatic shear failure in a clamped circular plate struck by a blunt projectile. Int J Impact Eng 2005;31:877–93.
[3] Nazeer MM, Khan MA, Naeem A, Haq A. Analysis of conical tool perforation of ductile metal sheets. Int J Mech Sci 2000;42:1391–403.
[4] Liu D, Stronge WJ. Ballistic limit of metal plates struck by blunt deformable missiles: experiments. Int J Solids Struct 2000;37:1403–23.
[5] Atkins AG, Khan MA, Liu JH. Necking and radial cracking around perforations in thin sheets at normal incidence. Int J Impact Eng 1998;21(7):521–39.
[6] Segletes SB. The erosion transition of tungsten-alloy long rods into aluminum targets. Int J Solids Struct 2007;44:2168–91.
[7] Balos S, Grabulov V, Sidjanin L, Pantic M, Radisavljevic I. Geometry, mechanical properties and mounting of perforated plates for ballistic application. Mater Des 2010;31:2916–24.
[8] Rusinek A, Rodriguez-Martinez JA, Zaera R, Klepaczko JR, Arias A, Sauvelet C. Experimental and numerical study on the perforation process of mild steel sheets subjected to perpendicular impact by hemispherical projectiles. Int J Impact Eng 2009;36:565–87.
[9] Klepaczko JR, Rusinek A, Rodríguez-Martínez JA, Pecherski RB, Arias A. Modelling of thermo-viscoplastic behaviour of DH-36 and Weldox 460-E structural steels at wide ranges of strain rates and temperatures, comparison of constitutive relations for impact problems. Mech Mater 2009;41:599–621.
[10] Dean J, Dunleavy CS, Brownb PM, Clyne TW. Energy absorption during projectile perforation of thin steel plates and the kinetic energy of ejected fragments. Int J Impact Eng 2009;36:1250–8.
[11] ASTM standard C33, 2003. Specification for concrete aggregates, ASTM International, West Conshohocken, PA; 2003. doi: 10.1520/C0033-03, www.astm.org.
[12] Durmuş A, Musayev E, Ülkü S. Measurement of bullet velocities by using a new digital velocity measurement equipment. J Defence Sci 2005;4(1):70–84 (in Turkish).
[13] Zukas JA, Nicholas T, Swift HF, Greszczuk LB, Curban DR. Impact dynamics. New York: John Wiley & Sons Inc.; 1982.
[14] Børvik T, Langseth M, Hopperstad OS, Malo KA. Perforation of 12 mm thick steel plates by 20 mm diameter projectiles with flat, hemispherical and conical noses. Part I: experimental study. Int J Impact Eng 2002;27:19–35.
[15] Radin J, Goldsmith W. Normal projectile penetration and perforation of layered targets. Int J Impact Eng 1998;7:229–59.
[16] Almohandes AA, Abdel-Kader MS, Eleiche AM. Experimental investigation of the ballistic resistance of steel–fiberglass reinforced polyester laminated plates. Compos Part B Eng 1996;27:447–58.
[17] Ben-Dor G, Dubinsky A, Elperin T. On the ballistic resistance of multi-layered targets with air gaps. Int J Solids Struct 1998;35:3097–103.
[18] Elek P, Jaramaz S, Mickovic D. Modeling of perforation of plates and multi-layered metallic targets. Int J Solid Struct 2005;42:1209–24.
[19] Gupta NK, Iqbal MA, Sekhon GS. Effect of projectile nose shape, impact velocity and target thickness on deformation behavior of layered plates. Int J Impact Eng 2008;35:37–60.
[20] Dey S, Børvik T, Teng X, Wierzbicki T, Hopperstad OS. On the ballistic resistance of double-layered steel plates: an experimental and numerical investigation. Int J Solids Struct 2007;44:6701–23.